Combustion and Flame 279 (2025) 114306

Contents lists available at ScienceDirect

Combustion and Flame

journal homepage: www.sciencedirect.com/journal/combustion-and-flame

Characterizing the influence of thermodiffusive effects on turbulent burning velocity of lean hydrogen/air mixtures using critically stretched laminar flames

Yiqing Wang [a,*,1], Andrei N. Lipatnikov [b], Zheng Chen [a]

[a] SKLTCS, HEDPS-CAPT, College of Engineering, Peking University, Beijing, 100871, China
[b] Department of Mechanics and Maritime Sciences, Chalmers University of Technology, Gothenburg, SE-412 96, Sweden

ARTICLE INFO

Keywords:
Turbulent burning velocity
Hydrogen
Thermodiffusive effects
Critically stretched laminar flames

ABSTRACT

This work focuses on characterizing the influence of thermodiffusive effects on turbulent burning velocity (S_T) of lean hydrogen/air mixtures, employing the so-called leading point concept. To this end, the flame characteristics of 1-D critically stretched laminar flames, including the flame consumption velocity and flame thickness, are extracted from two flame configurations: counter-flow twin premixed flames and spherically expanding flames. The former configuration is solely subject to strain-related stretch, whereas the latter configuration is subject to both strain-related and curvature-related stretches. Lean hydrogen/air mixtures are considered at a wide range of temperatures and pressures, addressed in recent direct numerical simulations (DNS) of turbulent, premixed, lean hydrogen/air flames (Wang et al., 2024). It is found that the critically stretched flame consumption velocities obtained from these two configurations are closely aligned, while the flame thickness obtained from the spherically expanding flames is substantially greater than that from the counter-flow twin premixed flames. Capabilities of these flame characteristics for capturing the thermodiffusive effects on S_T are demonstrated by incorporating these characteristics into fits to S_T dataset obtained from the aforementioned DNS study. Various definitions of flame thickness are also examined, with the thickness of fuel consumption zone showing the best performance. These findings support the leading point concept and imply that both critically strained planar flames and highly curved spherically expanding flames could be used to characterize the local burning state at the leading edges of turbulent lean premixed hydrogen flames.

Novelty and Significance Statement

The novelty of this research consists of comparing characteristics of critically stretched laminar flames, extracted from two flame configurations, i.e., twin planar counterflow flames and highly curved spherical flames. The results show that flame consumption velocities are approximately equal in these two extreme cases if complex chemistry of lean hydrogen burning is taken into account. Furthermore, for the first time to the authors' knowledge, the results (i) validate the leading point concept under conditions of fixed Karlovitz and Damköhler numbers, but different pressures and temperatures, (ii) indicate utility of characteristics of highly curved spherically expanding flames within the framework of this concept, and (iii) imply that the width of fuel consumption zone is better suited for evaluating thicknesses of critically stretched laminar flames (again within the framework of this concept). It is significant because prediction of high turbulent burning velocities, well documented in lean hydrogen/air mixtures, challenges the combustion community from the fundamental perspective and is of critical importance for the design and development of hydrogen-fueled engines.

1. Introduction

Due to the urgent need to replace traditional fossil fuels with renewable carbon-free fuels, there is a continuously growing interest in utilizing hydrogen (H_2) in various energy and propulsion systems [1,2]. Furthermore, burning hydrogen at lean conditions can decrease exhaust gas temperatures, and thus reduce NOx emissions. However, the application of lean premixed hydrogen combustion is still facing challenges, such as prediction of abnormally high turbulent burning rates, which

* Corresponding author
E-mail address: wangyiqing@pku.edu.cn (Y. Wang).
[1] The author is currently at Argonne National Laboratory.

https://doi.org/10.1016/j.combustflame.2025.114306
Received 11 March 2025; Received in revised form 16 June 2025; Accepted 17 June 2025
0010-2180/© 2025 The Combustion Institute. Published by Elsevier Inc. All rights are reserved, including those for text and data mining, AI training, and similar technologies.

have been well documented in the pioneering measurements by Karpov et al. [3,4] and in many subsequent experimental studies reviewed elsewhere [5], see also recent papers [6,7].

Many efforts were devoted to revealing the underlying mechanisms for this phenomenon, see review articles [5,8,9] and recent original papers [10–21]. In general, the abnormally high burning rate is widely accepted to result from local variations in the temperature and mixture composition due to the imbalance of reactant and heat fluxes to/from reaction zones wrinkled and stretched by turbulent eddies, which is known as thermodiffusive effects. Despite the significant progress on the understanding of such effects, accurate prediction for the high turbulent burning velocity (S_T) of lean premixed hydrogen flames remains a formidable challenge.

Several model strategies are developed to account for the influence of thermodiffusive effects on flame propagation. For example, Howarth and Aspden [22] proposed an empirical scaling model based on the second-order instability parameter that arises from classical linear stability analysis [23]. This model showed good performance on predicting the flame speed of laminar lean premixed hydrogen flames that are thermodiffusively unstable, and was supported in two recent numerical studies of turbulent burning [24,25]. In the context of applications, a simpler approach is to include the Lewis number (Le) in conventional scaling models for S_T to characterize the influence of thermodiffusive effects on it [26]. However, this method is purely empirical, and the fitting exponents of Le are rather scattered across different studies [26–30]. The present study focuses on another model approach, the so-called leading point concept pioneered by the Russian school [31,32].

According to the leading point concept, S_T is considered to be controlled by local characteristics of critically stretched, inherently laminar reaction zones localized to the leading edge of a turbulent flame brush [31,32]. Therefore, the flame properties of a critically stretched laminar flame are proposed to characterize the local structure of leading reaction zones in turbulent flows. The potential of this approach to predict the high S_T of lean mixtures containing H_2 was evidenced in several experimental [12–14,21,33,34] and numerical [35–38] studies. Specifically, by using characteristics of critically stretched laminar flames, four research groups [12,21,33,34] well parameterized their experimental data that showed a significant increase in S_T due to thermodiffusive effects. Note that those data were measured under a wide range of substantially different conditions (various flame configurations, fuels, equivalence ratios, turbulence characteristics). DNS data by Lee et al. [35] show that while the influence of thermodiffusive effects on conditioned profiles of fuel consumption rate, sampled from entire flame brushes, is mitigated with increasing rms turbulent velocity u', the opposite trend is observed both for S_T and for the counterpart conditioned profiles sampled from the flame-brush leading edges. Moreover, the latter profiles are close to results obtained from highly strained counter-flow twin laminar premixed flames. Other DNS data indicate that the highest (over entire computational domain) instantaneous fuel consumption rates are localized to flame-brush leading zones and oscillate weakly with time [35–37]. Furthermore, these highest rates are close to the highest fuel consumption rates in the aforementioned strained laminar flames [38].

More often, a critically stretched laminar flame highlighted by the leading point concept is associated with the aforementioned 1-D counter-flow twin premixed flame [12–14,21,32–35,38,39], where the flame is strained without any curvature as it is a planar flame. At the same time, many studies (e.g., [15,18,19]) have revealed that the local burning rate in a thermodiffusively unstable lean premixed hydrogen flame is closely related to the local curvature. Moreover, numerical simulations performed using one-step chemistry showed that the local burning rates reached in highly curved expanding spherical flames were much higher than in the counterpart counter-flow twin premixed flames [40]. Based on these results, highly curved laminar flames were proposed to be considered as an alternative model [5,41] of leading points in turbulent flows. Furthermore, recent complex-chemistry DNS studies [36–38] have shown that (i) despite the highest local fuel consumption rates sampled from different turbulent flames at various instants are always close to the local fuel consumption rates in the counterpart critically strained twin counterflow laminar flames, (ii) the local strain rates and the local flame curvatures measured in the points characterized by these highest local fuel consumption rates vary randomly and change their sign. These results could imply the lack of locality, i.e., strain rate or/and curvature evaluated in a single point within a reaction zone is insufficient to characterize local perturbations of the entire zone by turbulent eddies. These results could also suggest that comparably high fuel consumption rates could be reached in different configurations of critically stretched complex-chemistry laminar flames. In other words, in the case of complex chemistry, local consumption velocities in highly strained laminar flames could be close to local consumption velocities in highly curved laminar flames, contrary to the case of a single-step chemistry [40]. These points motivate us to investigate the utility of another conventional 1-D laminar flame configuration, i.e., a highly curved expanding spherical flame, for predicting high turbulent burning velocities in lean hydrogen flames adopting leading point concept.

In light of the above discussion, the objectives of this work are two-fold: (1) comparing characteristics of critically stretched counterflow twin premixed and spherically expanding flames, with complex chemistry being employed; (2) evaluating applicability of both sets of critically stretched flame characteristics for predicting high turbulent burning velocities in lean hydrogen/air mixtures.

The paper is organized as follows: in Section 2, a S_T dataset obtained recently from direct numerical simulations (DNS) [42] is briefly described; in Section 3, methodologies to extract characteristics of critically stretched laminar flames are presented for both counterflow twin premixed laminar flames and spherically expanding flames, followed by a comparison on the computed flame characteristics. In Section 4, the performance of these flame characteristics is evaluated by fitting the S_T dataset. Finally, findings are summarized in Section 5.

2. Turbulent burning velocity dataset

The turbulent burning velocity (S_T) dataset used in this work was recently obtained by Wang et al. [42] by running DNS. In those simulations, statistically planar turbulent flames of a lean premixed hydrogen/air mixture (the equivalence ratio $\phi = 0.6$) propagating in a 3-D box were considered. S_T was computed based on the fuel (H_2) consumption rate as:

$$S_T = \frac{1}{\rho_u Y_{\mathrm{H_2,u}} A_L} \int_{\Omega} \dot{\omega}_{\mathrm{H_2}} dV. \tag{1}$$

Here, ρ_u and $Y_{\mathrm{H_2},u}$ are the density and fuel mass fraction, respectively, in unburned mixture, A_L is the projected flame area on the streamwise direction, $\dot{\omega}_{\mathrm{H_2}}$ is the mass consumption rate of the fuel, Ω is the computational domain, and V is its volume. Details on the case setup (such as the initial and boundary conditions), as well as numerical methods, can be found elsewhere [42] and, thus, are not repeated here. A detailed chemical mechanism (9 species and 22 reactions) developed by Kéromnès et al. [43] was adopted in the DNS. The same mechanism is also used in the present 1-D laminar flame simulations.

Table 1 summarizes the thermochemical conditions and flame properties for all cases. Specifically, there are four groups of DNS cases with varying temperatures and pressures. In Groups 1 and 2, the unburned temperature (T_u) is increased from 300 to 641 K at atmospheric ($P = 1$ atm) and elevated ($P = 10$ atm) pressures, respectively. In Group 3, P is increased from 1 to 15 atm at fixed $T_u = 300$ K. In Group 4, T_u and P are increased simultaneously from ($P = 1$ atm, $T_u = 300$ K) to ($P = 15$ atm, $T_u = 641$ K) following an isentropic compression correlation. It is worth stressing that, for all cases, major non-dimensional characteristics of turbulent burning are fixed. Specifically, $u'/S_L = 2$ and $l_T/l_f = 1$. Here,

Table 1
Flame properties and non-dimensional parameters for DNS cases considered. S_L is the laminar flame speed, l_f is the thermal flame thickness, $\delta_{r,fw}$ and $\delta_{r,hw}$ are two reaction zone thicknesses, and Le_{eff} is the effective Lewis number. Definitions of l_f, $\delta_{r,fw}$ and $\delta_{r,hw}$ can be found in Section 3.

T_u [K]	P [atm]	S_L [m/s]	l_f [μm]	$\delta_{r,fw}$ [μm]	$\delta_{r,hw}$ [μm]	Le_{eff}	S_T/S_L
300	1	1.01	352	196	96	0.42	3.36
365	1	1.53	368	190	93	0.43	2.98
473	1	2.72	412	183	89	0.45	3.07
573	1	4.33	462	180	88	0.48	3.14
641	1	5.70	491	179	87	0.49	3.30
300	10	0.37	45	23	10	0.39	5.21
365	10	0.59	39	21	9.3	0.40	4.97
473	10	1.19	33	19	8.4	0.41	4.10
573	10	2.13	30	17	7.9	0.42	3.74
641	10	3.05	29	17	7.7	0.43	3.20
300	2	0.84	165	98	47	0.41	3.65
300	5	0.57	71	41	19	0.40	4.21
300	15	0.26	37	17	7.4	0.38	6.38
365	2	1.30	165	93	44	0.42	3.10
473	5	1.74	62	36	17	0.42	3.53
641	15	2.37	20	12	5.2	0.42	3.79

l_T is turbulence integral length scale, S_L and l_f are the laminar flame speed and thickness, respectively. Thus, the Damköhler number Da and Karlovitz number Ka remain constant, i.e., $Da = (l_T/l_f)/(u'/S_L) = 0.5$ and $Ka = (l_T/l_f)^{-0.5}(u'/S_L)^{1.5} = 2.8$. Therefore, all the flames are located at the same point in the Borghi-Peters regime diagram [44,45].

This design of a set of simulated cases has both advantages and disadvantages. On the one hand, Ka is moderate and constant. Therefore, influence of Karlovitz number on the magnitude of an increase in S_T/S_L due to thermodiffusive effects cannot be investigated. Nevertheless, this limitation of the present work appears to be of secondary importance, because the influence of Ka on S_T/S_L in lean hydrogen/air mixtures was already explored in other DNS studies [16,18,25,46,47]. On the other hand, variations in pressure and temperature at constant Da and Ka is the unique peculiarity of the present work, with this peculiarity offering new opportunities for studying thermodiffusive effects in turbulent flames. Indeed, conventional models of S_T, which allow only for u'/S_L and l_T/l_f (or equivalently, Da and Ka), will yield the same value of S_T/S_L in all cases. However, due to sensitivity of the magnitude of thermodiffusive effects to T_u and P, the ratio S_T/S_L varies considerably across different cases [42], as shown in Table 1. It is also worth stressing that various empirical models that allow for not only u'/S_L and l_T/l_f, but also Le [26–30] cannot predict significant variations in the computed S_T either, because the effective Lewis number Le_{eff} varies marginally at the thermochemical conditions considered in this work (equations used to calculate Le_{eff} are reported elsewhere [42]). For instance for Group 4, Le_{eff} remains unchanged when T_u and P are increased simultaneously, whereas S_T/S_L is significantly increased. The emphasized facts (constant u'/S_L, l_T/l_f, Da, or Ka, almost constant Le, but significantly different S_T/S_L) make the discussed dataset [42] particularly interesting for exploring capabilities of various models of S_T for predicting the thermodiffusive effects.

3. 1-D critically stretched laminar flames

Theoretically, the flame stretch, defined by the fractional rate of change of a flame surface element, can be decomposed into two components: one is the tangential strain rate which is related to the flow non-uniformity, and the other is the curvature stretch which is related to the propagating curved flame front. Therefore, two groups of 1-D critically stretched laminar flames are considered in this work: one is the 1-D counter-flow twin premixed flames which are solely subject to the tangential strain rate, and the other is the 1-D spherically expanding flames which are also subject to the curvature stretch.

3.1. 1-D counter-flow twin premixed flames

A series of 1-D counter-flow twin premixed flame is simulated for the same hydrogen/air mixture at the thermochemical conditions listed in Table 1 using Cantera [48]. The mixture-averaged transport model without Soret effect is employed as in the DNS [42]. The critical stretch rates are reached by gradually increasing the inlet flow velocity until the flame is quenched. The flame consumption velocity $S_{c,str}$ is computed using Eq. (1) in a 1-D planar coordinate framework, and the thermal flame thickness $l_{f,str}$ of the strained flame is evaluated as follows:

$$l_{f,str} = \frac{T_b - T_u}{|\nabla T|_{max}}, \tag{2}$$

where T_b is the burned gas temperature. Eq. (2) is also adopted to determine the thermal thickness l_f of the unstrained flame. The flame stretch rate K is calculated using the following simplest formula

$$K = \frac{U_{in}}{L}, \tag{3}$$

because exact values of K are of minor importance for the present study. Here, U_{in} is the inlet velocity and L is the domain length. The subscript "str" means the flame properties are obtained from a ***strained*** flame, i.e., 1-D counter-flow twin premixed flame.

Figs. 1 and 2 show variations of normalized flame consumption velocity ($S_{c,str}/S_L$) and corresponding normalized thermal flame thickness ($l_{f,str}/l_f$) with normalized flame stretch ($K * l_f/S_L$) at different pressures and temperatures. In most cases, $S_{c,str}$ is increased with increasing K and reaches a peak value $S_{c,str}^{max}$ at a high, near-critical stretch rate, with the flame being quenched by a slightly higher strain rate. The thickness $l_{f,str}$ is monotonically decreased with increasing K. Following the leading point concept, these peak values $S_{c,str}^{max}$ and the corresponding flame thickness $l_{f,str}^{max}$ ($l_{f,str}$ at the flame stretch corresponding to $S_{c,str}^{max}$, marked with squares in Fig. 2) will be used when analyzing the DNS data on S_T for lean premixed hydrogen/air flames. Note that for cases with elevated temperature but atmospheric pressure (i.e., T_u = 473–641 K, P = 1 atm), $S_{c,str}$ of stretched flame is always smaller than S_L, as shown in Fig. 1(a). This indicates that these flames are not accelerated by thermodiffusive effects. Therefore, for these flames, $S_{c,str}^{max} = S_L$ and $l_{f,str}^{max} = l_f$ are used following [5,21,34]. Note that the decrease in $S_{c,str}/S_L$ with increasing strain rate, observed at T_u = 473–641 K and P = 1 atm, is typical for hydrocarbon-air mixtures characterized by Lewis numbers close to or larger than unity. This trend is associated with positive Markstein numbers predicted for such mixtures by various activation energy asymptotic theories reviewed elsewhere [5]. Negative slopes of the three discussed curves (T_u = 473, 573, and 641 K) at low strain rates indicate that Markstein numbers are positive in these cases also. An increase in Markstein number due to an increase in T_u was also reported in another recent numerical study of lean H_2/air strained laminar flames [49]. This trend is associated with a decrease in Zel'dovich number Ze with increasing T_u at atmospheric pressure [50] (see Supplementary Material for Ze values at different conditions). This results in decreasing magnitude of the Le-dependent contribution to Markstein number, which is proportional to $Ze(Le - 1)$ [23] and is negative in lean hydrogen/air mixtures.

Apart from the thermal flame thickness l_f, the reaction zone thickness δ_r is also recognized as a characteristic length scale of laminar flames. Therefore, in this work, the suitability of δ_r to characterizing the influence of thermodiffusive effects on S_T is also explored. The thickness δ_r could be evaluated based on either fuel consumption rate (FCR) or heat release rate (HRR). DNS studies by Lee et al. [36,37] indicated that the extreme (highest) HRR values exhibit strong temporal fluctuations, while the extreme FCR values fluctuate weakly and are close at different turbulent Karlovitz numbers. These findings suggest that FCR is more relevant to the leading point concept than HRR. Therefore, the FCR-based δ_r is adopted in this work. Specifically, two definitions are considered:

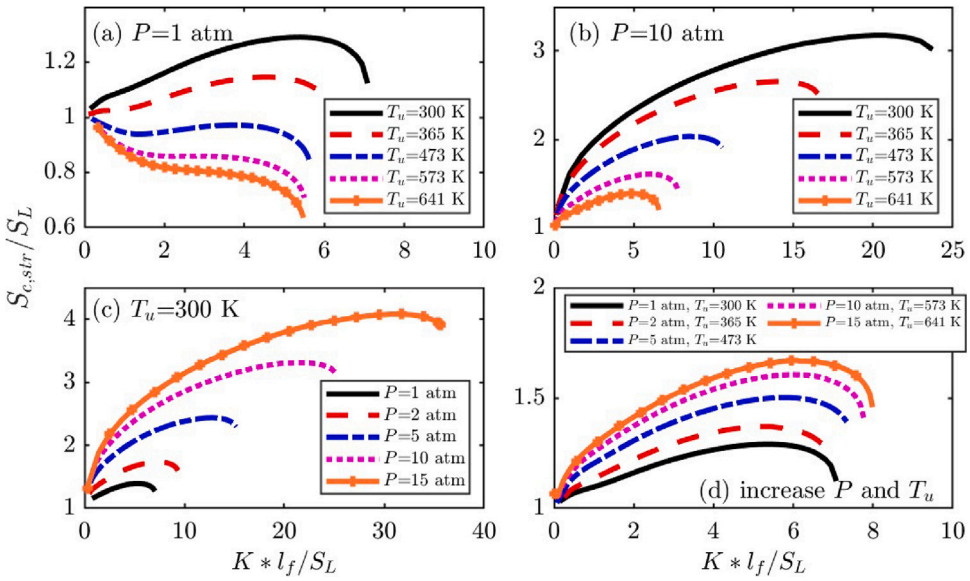

Fig. 1. Variation of normalized flame consumption velocity $S_{c,str}/S_L$ with normalized stretch rate $K * l_f/S_L$ in twin premixed counterflow flames.

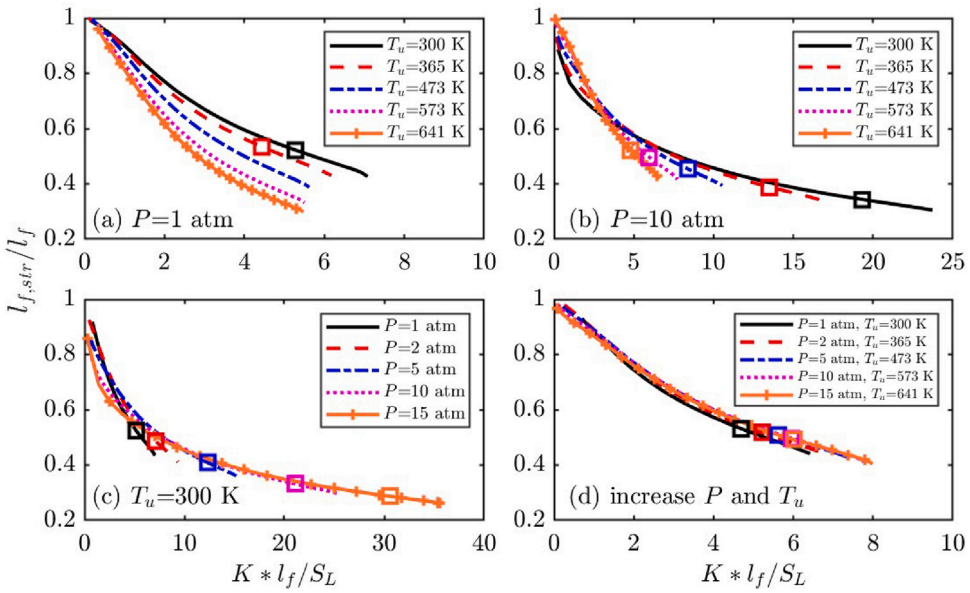

Fig. 2. Variations of normalized flame thickness $l_{f,str}/l_f$ with normalized stretch rate $K * l_f/S_L$ in twin premixed counterflow flames. Squares represent $l_{f,str}$ at the flame stretch corresponding to $S_{c,str}^{max}$, i.e., $l_{f,str}^{max}$.

- $\delta_{r,fw}$, defined as the ***full width*** at half maximum (FWHM) of the FCR profile, which is the width of the region where the local FCR exceeds 50% of its peak value;
- $\delta_{r,hw}$, defined as the **half *width*** at half maximum (HWHM) of the FCR profile, measured upstream of the maximum, i.e., the left half of FWHM.

Fig. 3 exemplarily shows variations of $\delta_{r,fw,str}$ and $\delta_{r,hw,str}$ with the stretch rate K for the case with T_u = 300 K and P = 1 atm. The consumption velocity $S_{c,str}$ is also presented for reference. Unlike $l_{f,str}$, which shows a monotonically decreasing trend with K, $\delta_{r,fw,str}$ varies non-monotonically at high K. Specifically, $\delta_{r,fw,str}$ decreases with K at low-to-moderate K, but then begins to increase after reaching a certain threshold of K. This results in a local minimum of $\delta_{r,fw,str}$ (see point "f1" in Fig. 3). As K continues increasing, $\delta_{r,fw,str}$ eventually experiences a sharp drop when K is sufficiently close to the extinction limit. Consequently, there is a local maximum of $\delta_{r,fw,str}$ (see point "f3"). The $\delta_{r,fw,str}$ corresponding to the maximum $S_{c,str}$ lies between f1 and f3 and is marked as "f2".

To understand this abnormal trend of $\delta_{r,fw,str}$ at high K, Fig. 4 examines the flame structures associated with points f1, f2 and f3. Specifically, Fig. 4 shows spatial profiles of FCR ($\dot{\omega}_F$), temperature (T), and mole fraction of H_2 (X_{H_2}). As K increases, the peak temperature decreases, and the amount of unburned H_2 increases, suggesting that the combustion process is substantially influenced by the boundary conditions on the burned gas side. In other words, the reaction zone interacts directly with the boundary, where gradients of temperature and species concentrations vanish. Consequently, the gradient of $\dot{\omega}_F$ is also zero, leading to a flattening of the $\dot{\omega}_F$ profile near the boundary and a broadening of the reaction zone. With higher K, the reaction zone is more influenced by the boundary, resulting in larger $\delta_{r,fw,str}$. This explains the observed increasing trend of $\delta_{r,fw,str}$ with K. Regarding the final sharp decrease of $\delta_{r,fw,str}$ at extremely high K, the explanation

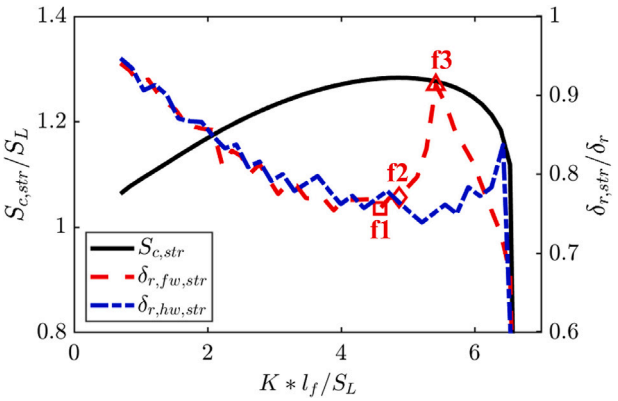

Fig. 3. Variations of normalized $S_{c,str}/S_L$, $\delta_{r,fw,str}/\delta_{r,fw}$ and $\delta_{r,hw,str}/\delta_{r,hw}$ with normalized stretch rate $K * l_f/S_L$ in twin premixed counterflow flames. T_u = 300 K and P = 1 atm.

is straightforward: when the flame approaches extinction, the reaction zone is greatly reduced.

The above results suggest that the abnormal trend of $\delta_{r,fw,str}$ at high K is primarily due to the influence of the boundary. This observation has motivated us to use $\delta_{r,hw,str}$ as an alternative. By definition, $\delta_{r,hw,str}$ measures the thickness of the half reaction zone farther from the boundary, making $\delta_{r,hw,str}$ less susceptible to boundary effects compared to $\delta_{r,fw,str}$. This can also be seen in Fig. 4(a), where no significant differences are observed in the left haft of $\dot{\omega}_F$ profiles across different flames. As a result, the non-monotonic trend of $\delta_{r,hw,str}$ with K is much less pronounced than that of $\delta_{r,fw,str}$, as shown in Fig. 3. It is also worth mentioning that the curves of $\delta_{r,fw,str}$ and $\delta_{r,hw,str}$ are nearly overlapping at low K associated with the initial monotonic decrease in the thickness with the strain rate.

Figs. 5 and 6 show variations of normalized $\delta_{r,fw,str}$ and $\delta_{r,hw,str}$ with stretch, at different pressures and temperatures. As shown in Fig. 5, $\delta^{max}_{r,fw}$ can belong to different branches of the $\delta_{r,fw,str}(K)$-curve, namely, the initially decreasing branch, the intermediately increasing branch, and the final sharply decreasing branch, depending on the specific conditions. This variability introduces significant uncertainties in determination of $\delta_{r,fw,str}$. In contrast, $\delta^{max}_{r,hw,str}$ is typically close to the local minimum of the $\delta_{r,fw,str}(K)$-curve (or is associated with the initially decreasing branch of the curve). This fact substantially reduces the ambiguity in determining $\delta^{max}_{r,hw,str}$ and makes this thickness more suitable for evaluating S_T using leading point concept.

3.2. 1-D spherically expanding flames

The 1-D spherical flame propagating in a closed vessel is simulated using the in-house code A-SURF [51,52]. The length of simulation domain is set equal to 4 cm so that the pressure increase is negligible throughout the simulation, as shown in the Supplementary Material. The unburned mixture is initially static and spatially uniform. A hot kernel with a radius of R_H, filled with equilibrium combustion products, is introduced at the center to initiate a flame kernel. Unsteady, compressible Navier–Stokes, energy, and species transport equations for a multi-component reactive flow are solved in a spherical coordinate framework using the finite volume method [51,52]. The same transport model as in the case of the twin flames is employed. To accurately and efficiently resolve the flame front structure, the dynamically adaptive mesh refinement (AMR) is applied based on the temperature gradient. Consequently, the minimum mesh size ranges from 0.5 to 4 μm across different cases, ensuring that there are sufficient grid points within the reaction zone. A grid convergence study is provided in the Supplementary Material. More details on governing equations, numerical schemes, and code validation can be found in Ref. [51].

Unlike the counter-flow twin premixed flame, the spherically expanding flame is unsteady, and the transient flame propagation process is influenced by the initial conditions (e.g., the ignition kernel), especially during the early stage. Note that the early flame propagation is of particular interest in this work, because the flame radius is small and the curvature stretch is high during this stage. Therefore, in order to reduce the influence of the initial conditions and to avoid the ambiguity of flame properties obtained from spherically expanding flames, the following three steps are adopted to extract the flame consumption velocity and thickness from 1-D critically stretched spherical flames.

- First, different values of ignition kernel radius R_H are tested to find the critical R_H (denoted as $R_{H,c}$), below which the flame cannot propagate, i.e., the initial kernel shrinks. It is expected that with smaller R_H, the curvature stretch that the flame undergoes during the early stage would be higher.
- Second, based on the case with $R_H = R_{H,c}$, time-dependencies of the flame consumption velocity $S_{c,curv}$, the thermal flame thickness $l_{f,curv}$, and the two reaction zone thicknesses $\delta_{r,fw,curv}$ and $\delta_{r,hw,curv}$, are recorded, where the subscript "curv" means they are obtained from a ***curved*** flame.
- Third, a peak value (denoted as $S^{max}_{c,curv}$) is extracted from the time history of $S_{c,curv}$. At the same instant, the flame thicknesses $l^{max}_{f,curv}$, $\delta^{max}_{r,fw,curv}$ and $\delta^{max}_{r,hw,curv}$, are then extracted.

To explicitly show how $S^{max}_{c,curv}$, $l^{max}_{f,curv}$, $\delta^{max}_{r,fw,curv}$ and $\delta^{max}_{r,hw,curv}$ are obtained following the three steps mentioned above, results for the case with T_u = 300 K and P = 1 atm are presented in Figs. 7 and 8 as an example. The results for the other cases are provided in the Supplementary Material. Specifically, Fig. 7 shows the temporal evolution of the flame radius (R_f, defined as the maximum heat release rate position) at three different R_H, i.e., R_H = 0.72, 0.76, and 0.8 mm. It is seen that for R_H = 0.76 mm, the flame is successfully ignited, while for R_H = 0.72 mm, the ignition fails. Therefore, it can be deduced that the critical R_H, i.e., $R_{H,c}$, is equal to 0.76 mm with less than 6% uncertainty. Then, Fig. 8 shows the temporal evolution of the R_f, $S_{c,curv}$, $l_{f,curv}$, $\delta_{r,fw,curv}$ and $\delta_{r,hw,curv}$ at $R_H = R_{H,c}$ = 0.76 mm. Two peaks are observed for the $S_{c,curv}$ curve. However, the first peak is largely influenced by the ignition kernel, and the flame is still not fully developed. Therefore, the second peak of $S_{c,curv}$ is defined as $S^{max}_{c,curv}$, and $l^{max}_{f,curv}$ is extracted from $l_{f,curv}$ curve at the same instant. $\delta^{max}_{r,fw,curv}$ and $\delta^{max}_{r,hw,curv}$ are obtained in the same way. All $S^{max}_{c,curv}$, $l^{max}_{f,curv}$, $\delta^{max}_{r,fw,curv}$ and $\delta^{max}_{r,hw,curv}$ are marked with pentagrams in Fig. 8.

Note that in the counter-flow twin premixed flames, $S_{c,str}$ is found to be always smaller than S_L at $T_u \geq 473$ K and atmospheric pressure. This phenomenon is also observed in the spherically expanding flames. For example, Fig. 9 shows the temporal evolution of R_f, $S_{c,curv}$, and all flame thicknesses at $R_H = R_{H,c}$ for the case with T_u = 573 K and P = 1 atm. It is seen that the peak of $S_{c,curv}$ is smaller than S_L (shown in a horizontal dashed line). Therefore, at this condition, $S^{max}_{c,str} = S_L$, $l^{max}_{f,str} = l_f$, $\delta^{max}_{r,fw,curv} = \delta_{r,fw}$ and $\delta^{max}_{r,hw,curv} = \delta_{r,hw}$ are specified, following the same strategy used previously for the counter-flow twin premixed flames.

3.3. Comparison on flame properties obtained from different critically stretched laminar flames

In this subsection, critically stretched flames' properties computed in the stationary counter-flow and expanding spherical cases are compared at different temperatures and pressures.

Fig. 10 shows $S^{max}_{c,str}$ and $S^{max}_{c,curv}$, with both quantities being normalized with the same S_L. Both $S^{max}_{c,str}$ and $S^{max}_{c,curv}$ are decreased with increasing T_u, while are increased with increasing P. This is consistent with results of previous simulations of twin counter-flow flames [42,49] and implies that the thermodiffusive effects are enhanced at high pressures but suppressed at high temperatures. For the present study goals,

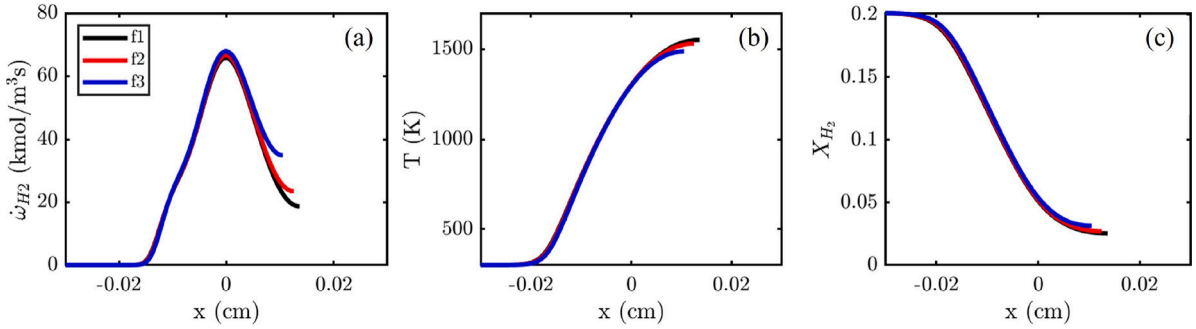

Fig. 4. Spatial profiles of FCR (a), temperature (b), and mole fraction of H_2 (c) for twin premixed counterflow flames at three strain rates associated with points f1, f2, and f3. T_u = 300 K and P = 1 atm.

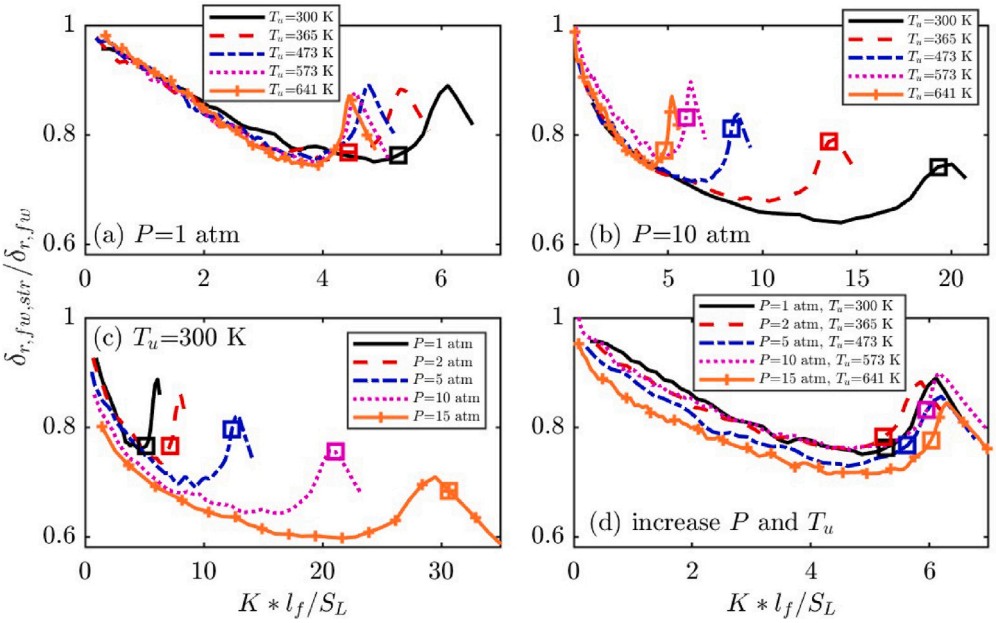

Fig. 5. Variation of normalized reaction zone thickness $\delta_{r,fw,str}/\delta_{r,fw}$ with normalized stretch rate $K * l_f/S_L$ in twin premixed counterflow flames. Squares represent $\delta_{r,fw,str}$ at the flame stretch corresponding to $S^{max}_{c,str}$, i.e., $\delta^{max}_{r,fw,str}$.

it is of the most interest that $S^{max}_{c,str}$ and $S^{max}_{c,curv}$ are close to each other across all thermochemical conditions, although the two consumption velocities are obtained from different flame configurations, where the flame is subject to different types of flame stretch. This finding could imply that the highest local flame consumption velocity is an intrinsic property of a complex-chemistry lean hydrogen–air mixture and can be reached in variously perturbed laminar flames. It is worth recalling that $S^{max}_{c,curv}$ is substantially higher than $S^{max}_{c,str}$ in the case of a single-case chemistry and a low Lewis number [40].

In contrast, as shown in Fig. 11, considerable difference is observed between the normalized thermal flame thicknesses $l^{max}_{f,str}/l_f$ and $l^{max}_{f,curv}/l_f$. Specifically, $l^{max}_{f,str}/l_f$ is smaller than $l^{max}_{f,curv}/l_f$ at most conditions. In addition, the dependence of the thermal flame thickness on temperature and pressure is also different from the flame consumption velocity. With increasing T_u, the thermal flame thickness is increased, while with increasing P, it is decreased.

The results reported in Figs. 10 and 11 are presented in another form in Fig. 12. This figure clearly reveals a negative correlation between the consumption velocities and thicknesses of critically stretched flames. Note that, for the spherically expanding flame, the normalized thickness $l^{max}_{f,curv}/l_f$ smoothly decreases from unity as $S^{max}_{c,curv}/S_L$ is increased, while for the counter-flow twin premixed flame, a sharp drop in the thickness is observed.

Similar analyses can also be performed for the reaction zone thickness. Fig. 13 compares reaction zone thicknesses of the critically stretched flames, obtained using two different definitions (“fw” vs. “hw”) from two different flame configurations (“str” vs. “curv”). Two observations are worth noting. First, the normalized $\delta^{max}_{r,fw,curv}$ and $\delta^{max}_{r,hw,curv}$ are almost identical, while there are noticeable differences between normalized $\delta^{max}_{r,fw,str}$ and $\delta^{max}_{r,hw,str}$. This indicates that, unlike the counter-flow twin premixed flames, the critically stretched reaction zone thickness for spherically expanding flames is not influenced by boundary conditions, making it less sensitive to the definition of δ_r. Second, when using the full width definition of δ_r, the results obtained from counter-flow twin premixed flames and spherically expanding flames are generally closer, but the differences are larger when the half width definition of δ_r is applied. Nevertheless, the differences are sufficiently small even in the latter (“hw”) case.

Finally, Fig. 14 examines correlations between the reaction zone thickness and consumption velocity of critically stretched flames. The data points obtained from spherically expanding flames clearly show a negative correlation between the reaction zone thickness and flame consumption velocity, regardless of the definition of δ_r. However, when using the counter-flow twin premixed flame configuration, the results from the full width definition do not show a clear correlation. This is due to large uncertainties introduced during the determination of $\delta^{max}_{r,fw,str}$. In contrast, the results obtained adopting the half width

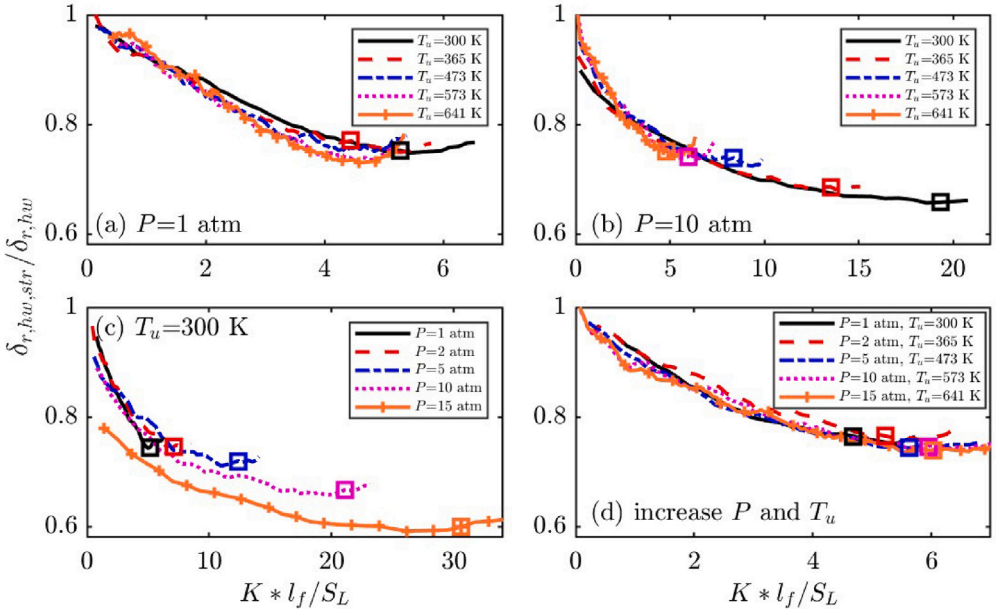

Fig. 6. Variation of normalized reaction zone thickness $\delta_{r,hw,str}/\delta_{r,hw}$ with normalized stretch rate $K * l_f/S_L$ in twin premixed counterflow flames. Squares represent $\delta_{r,hw,str}$ at the flame stretch corresponding to $S_{c,str}^{max}$, i.e., $\delta_{r,hw,str}^{max}$.

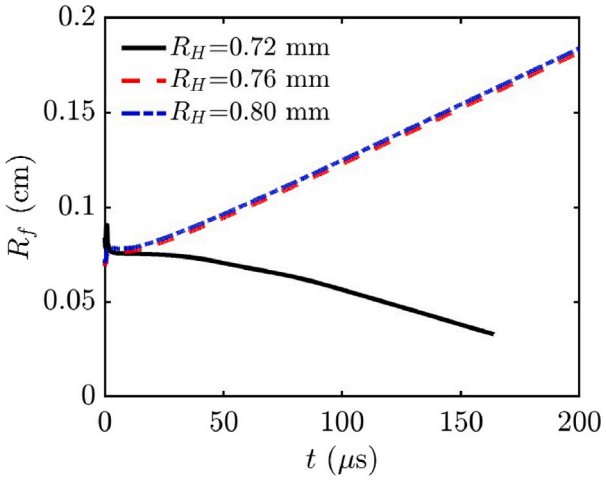

Fig. 7. Temporal evolution of the flame radius (R_f) induced by different ignition kernel sizes (R_H). T_u = 300 K and P = 1 atm.

definition exhibit a similar negative correlation to that observed in spherically expanding flames.

4. Scaling of turbulent burning velocity

Regarding an empirical model of S_T, the following general power-law scaling relation is considered:

$$\frac{S_T}{u'} \propto \left(\frac{u'}{S_L}\right)^{\alpha} \left(\frac{l_T}{l_f}\right)^{\beta}. \tag{4}$$

While many models are based on Ka, Da, or the turbulent Reynolds number Re_T, they are subsumed by Eq. (4), because Ka, Da, and Re_T are functions of u'/S_L and l_T/l_f if variations in the flame Reynolds number $Re_F = S_L l_f/\nu$ are disregarded. Here, ν is unburned gas viscosity.

Within the framework of leading point concept, S_L and l_f in Eq. (4) should be substituted with the corresponding flame properties obtained from the critically stretched flames [5,21]. Therefore, Eq. (4) is changed to:

$$\frac{S_T}{u'} = a\left(\frac{u'}{S_c^{max}}\right)^{\alpha}\left(\frac{l_T}{l_f^{max}}\right)^{\beta} \tag{5}$$

where a is a constant, and S_c^{max} and l_f^{max} represent the consumption velocity and thickness of a critically stretched flame. Note that the critically stretched flame can be either a counter-flow twin premixed flame or a spherically expanding flame, and the flame thickness can be either the thermal flame thickness or the reaction zone thickness. This results in six different combinations of S_c^{max} and l_f^{max}, leading to six empirical models in total.

To determine the optimal values of the power exponents α and β, a methodology used in Refs. [21,34] is directly adopted. First, the ratio $r = \beta/\alpha$ is varied with the step size of $\Delta r = 0.01$. Next, a least square fit is applied to all S_T data to determine $a(r)$ and $\alpha(r)$ for each value of r. Finally, the specific ratio r_m and the corresponding $a(r_m)$ and $\alpha(r_m)$ that minimize the following error function

$$\epsilon = \Sigma[\ln(S_T/u') - \ln(a) - \alpha\ln(u'/S_c^{max}) - \beta\ln(l_T/l_f^{max})]^2 \tag{6}$$

are selected.

Fig. 15 presents the obtained relationships between $\ln(S_T/u')$ and $\ln[(u'/S_c^{max})(l_T/l_f^{max})^{r_m}]$. It can be observed that, across all six combinations of S_c^{max} and l_f^{max}, the proposed scaling parameter effectively collapses the DNS data points onto a linear function with a goodness of data fitting (R^2) higher than 0.92. It is important to note that, for all DNS cases considered, u'/S_L and l_T/l_f are held constant. Therefore, the conventional empirical Eq. (4) will yield the same value of S_T/u' for all cases. Moreover, significant variations in S_T/u' computed in the DNS are difficult to link with small variations in Le from case to case. In this regard, the good performance of Eq. (5) supports the leading point concept by showing that S_T of lean premixed hydrogen/air flames at a wide range of temperatures and pressures can be accurately predicted highlighting characteristics of critically stretched laminar premixed flames.

Table 2 summarizes the fitted values of a, α, and β in Eq. (5), used to create Fig. 15, as well as the corresponding coefficients of determination R^2, for each combination of S_c^{max} and l_f^{max}. When the reaction zone thickness is used as the characteristic flame length scale,

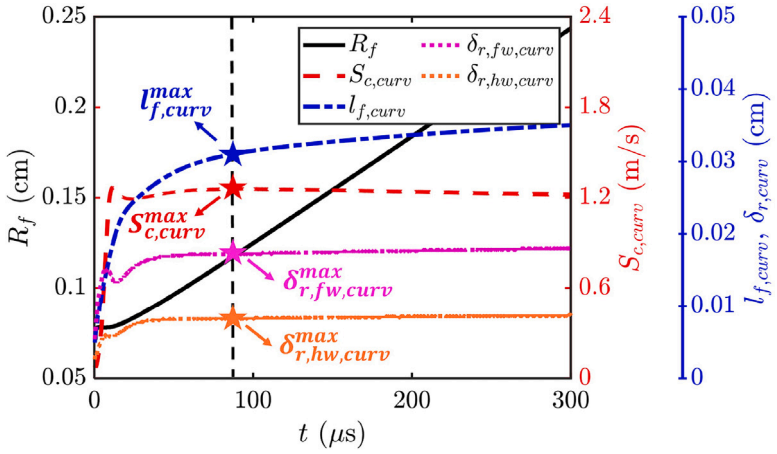

Fig. 8. Temporal evolution of the flame radius (R_f), flame consumption velocity ($S_{c,curv}$), thermal flame thickness ($l_{f,curv}$), and reaction zone thicknesses $\delta_{r,fw,curv}$ and $\delta_{r,hw,curv}$ at $R_H = R_{H,c}$. T_u = 300 K and P = 1 atm.

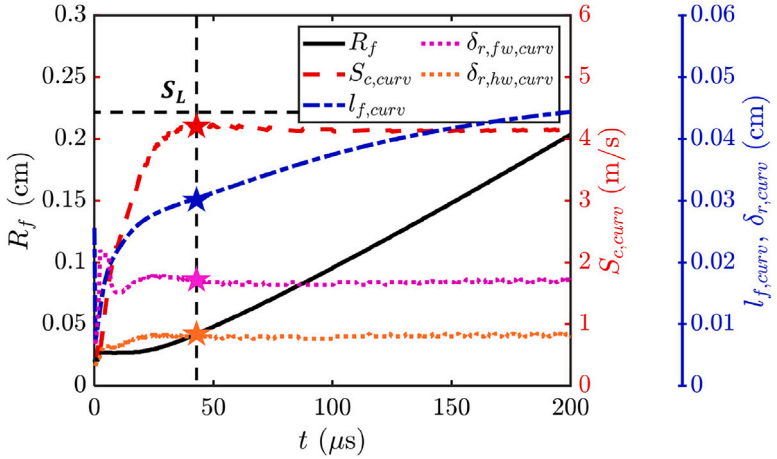

Fig. 9. Temporal evolution of the flame radius (R_f), flame consumption velocity ($S_{c,curv}$), flame thickness ($l_{f,curv}$), and reaction zone thicknesses $\delta_{r,fw,curv}$ and $\delta_{r,hw,curv}$ at $R_H = R_{H,c}$. T_u = 573 K and P = 1 atm.

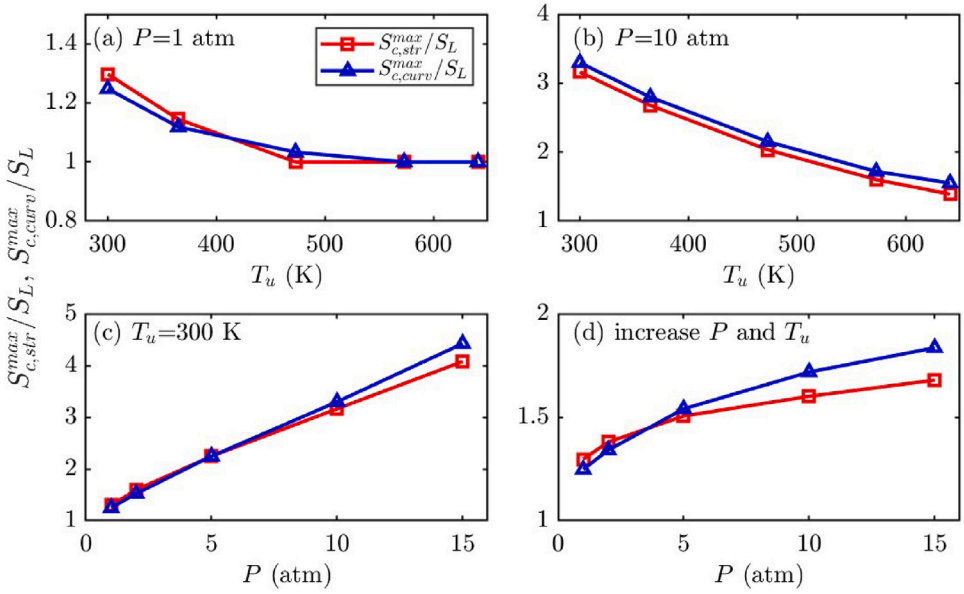

Fig. 10. Variations of $S^{max}_{c,str}/S_L$ and $S^{max}_{c,curv}/S_L$ with T_u and P.

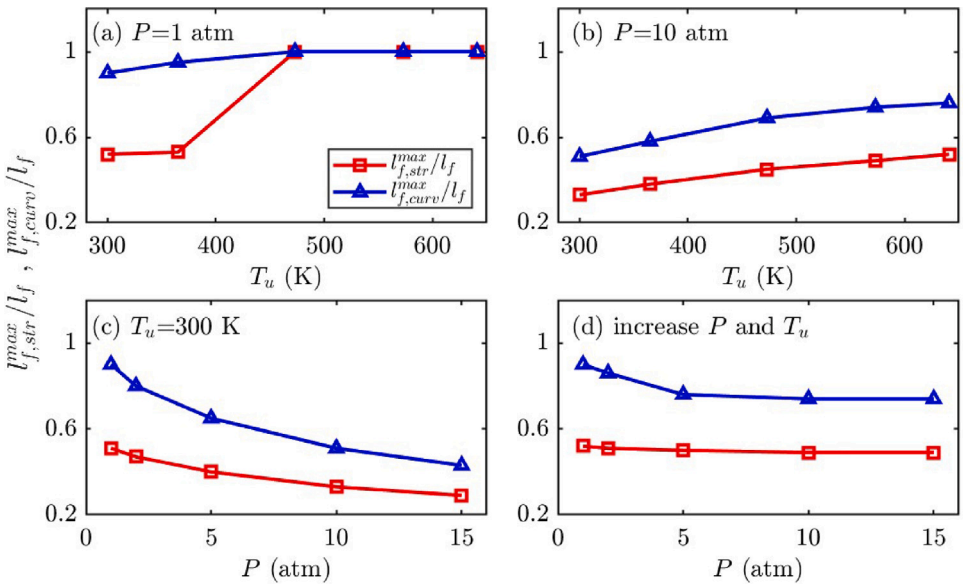

Fig. 11. Variations of $l_{f,str}^{max}/l_f$ and $l_{f,curv}^{max}/l_f$ with T_u and P.

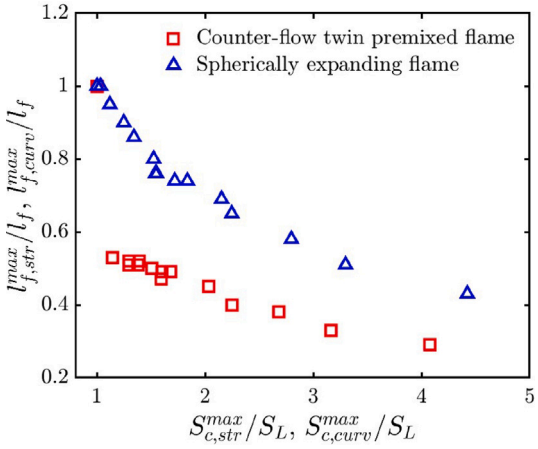

Fig. 12. Variations of normalized thermal flame thickness with normalized flame consumption speed, extracted from the two types of critically stretched flames.

the exponent β is positive, in line with positive values of l_T/l_f reported in previous studies, e.g., [28,29,53]. In contrast, negative β is observed when the thermal flame thickness is employed. In addition, β exhibits strong sensitivity to the flame configuration when using the thermal flame thickness, while β remains nearly identical across two flame configurations when using the reaction zone thickness. Based on these observations, the reaction zone thickness is preferred as the characteristic flame length scale for modeling S_T. Among the two definitions of reaction zone thickness considered, (1) the half width definition is less affected by boundary conditions in the counter-flow twin premixed flames, and (2) empirical models employing the half width definition achieve higher R^2 values. Therefore, $\delta_{r,hw,str}^{max}$ and $\delta_{r,hw,curv}^{max}$ are recommended for the modeling purpose.

It is worth noting that the length scale ratio was neglected in several previous applications of the leading point concept to parameterizing experimental data [12–14,33]. Following this approach, the empirical models that do not account for the flame thickness are also considered in this work. By manually setting $\beta = 0$, the following two models that only include u'/S_c^{max} are obtained:

$$\frac{S_T}{u'} = 2.08\left(\frac{u'}{S_{c,str}^{max}}\right)^{-0.50}, \tag{7}$$

and:

$$\frac{S_T}{u'} = 2.03\left(\frac{u'}{S_{c,curv}^{max}}\right)^{-0.48}. \tag{8}$$

Table 2
Constants used in Eq. (5) for all combinations of S_c^{max} and l_f^{max}.

Model#	Flame properties	a	α	β	R^2	Fig.#
1	$S_{c,str}^{max}$, $l_{f,str}^{max}$	2.61	−0.72	−0.28	0.96	Fig. 15(a)
1	$S_{c,curv}^{max}$, $l_{f,curv}^{max}$	2.08	−0.51	−0.06	0.92	Fig. 15(b)
2	$S_{c,str}^{max}$, $\delta_{r,fw,str}^{max}$	1.58	−0.47	0.31	0.95	Fig. 15(c)
2	$S_{c,curv}^{max}$, $\delta_{r,fw,curv}^{max}$	1.57	−0.42	0.32	0.98	Fig. 15(d)
3	$S_{c,str}^{max}$, $\delta_{r,hw,str}^{max}$	1.04	−0.37	0.40	0.96	Fig. 15(e)
3	$S_{c,curv}^{max}$, $\delta_{r,hw,curv}^{max}$	1.11	−0.39	0.39	0.98	Fig. 15(f)
4	only $S_{c,str}^{max}$	2.08	−0.50	–	0.92	Fig. 16(a)
4	only $S_{c,curv}^{max}$	2.03	−0.48	–	0.91	Fig. 16(b)

Fig. 16 shows that these two simplified models still perform well on characterizing S_T. Although the R^2 values are lower compared to those obtained using $\delta_{r,hw,str}^{max}$ and $\delta_{r,hw,curv}^{max}$, they remain above 0.9. These results highlight the robustness of incorporating the leading point concept into the empirical modeling of S_T, even when the flame thickness is not explicitly considered.

5. Conclusions

Inspired by leading point concept of premixed turbulent combustion, characteristics of 1-D critically stretched laminar flames, including the flame consumption velocity and differently defined flame thicknesses, were investigated using two canonical flame configurations: counter-flow twin premixed flames and spherically expanding flames. Lean premixed hydrogen/air mixtures were considered across a wide range of temperatures and pressures, matching the thermochemical conditions addressed in recent direct numerical simulations [42]. The results show that the critically stretched flame consumption velocities obtained from these two flame configurations are closely aligned, exhibiting a decreasing trend with temperature while an increasing trend

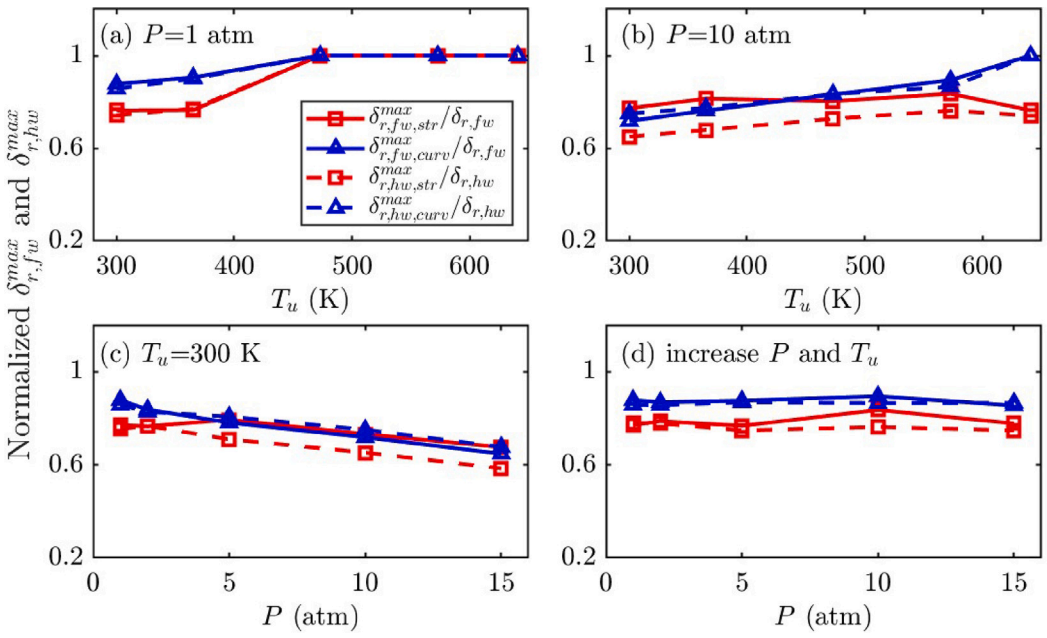

Fig. 13. Variations of normalized reaction zone thickness of critically stretched flames with T_u and P. Results computed using the full width and half width definitions are plotted in solid and dashed lines, respectively.

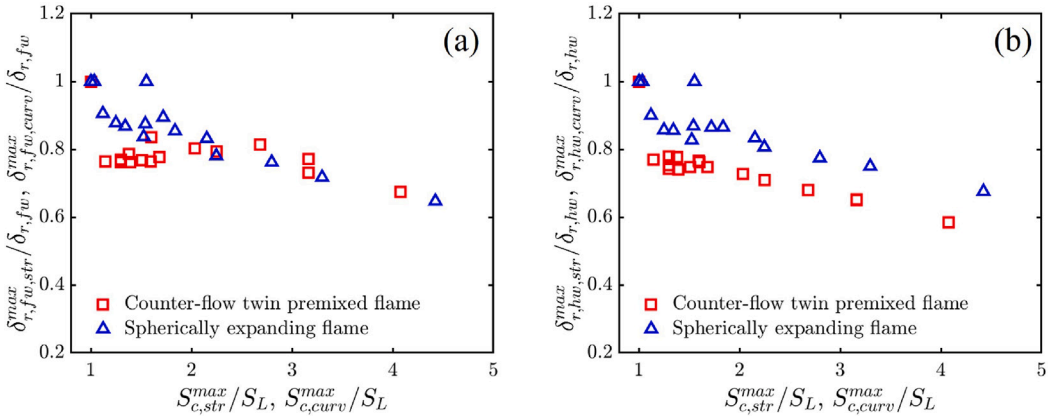

Fig. 14. Variations of normalized reaction zone thickness with normalized flame consumption speed, extracted from critically stretched flames. (a) full width, (b) half width.

with pressure. In contrast, the critically stretched flame thicknesses show an opposite dependence on temperature and pressure compared to the flame consumption velocity. In addition, the thermal flame thickness obtained from the spherically expanding flames is considerably greater than that from the counter-flow twin premixed flames.

The ability of these flame characteristics to capture variations of the magnitude of thermodiffusive effects on S_T with pressures and temperatures was assessed by incorporating the aforementioned characteristics into an empirical scaling model for the S_T dataset obtained in the aforementioned DNS study [42]. Various definitions of stretched laminar flame thickness were also examined. The use of characteristics of critically stretched laminar flames, obtained from both flame configurations, allowed us to well parameterize variations of the computed S_T with pressures and temperatures. Among the flame thickness definitions considered, the reaction zone thickness defined as the half width at half maximum of the fuel consumption rate profile, was found to outperform the others, as it yielded more robust model constants and better performance.

These findings not only support the leading point concept of premixed turbulent combustion, but also underscore that the spherically expanding flame can also serve as a good candidate of the critically stretched laminar flame to characterize the local burning rate at the leading edge of a turbulent lean hydrogen flame. These findings also imply that approximately the same highest local flame consumption velocity could be reached in various configurations of strongly perturbed complex-chemistry lean hydrogen–air laminar flames. Future work could extend this analysis to conditions more representative of practical engine environments.

While the present study is restricted to a single moderate value of Karlovitz number, the reported results considered jointly with results of two recent applications of leading point concept to parameterizing experimental data obtained from expanding statistically spherical $H_2/O_2/N_2$ (ϕ = 0.45) flames [21] and statistically stationary $NH_3/H_2/N_2/O_2$ ($0.355 \le \phi \le 0.765$) jet flames [34] show a wide range of the concept utility, e.g., Karlovitz number was varied from 0.6 to 1670 in the latter measurements. It is also worth noting that characteristics of critically stretched laminar flames, adopted to parameterize

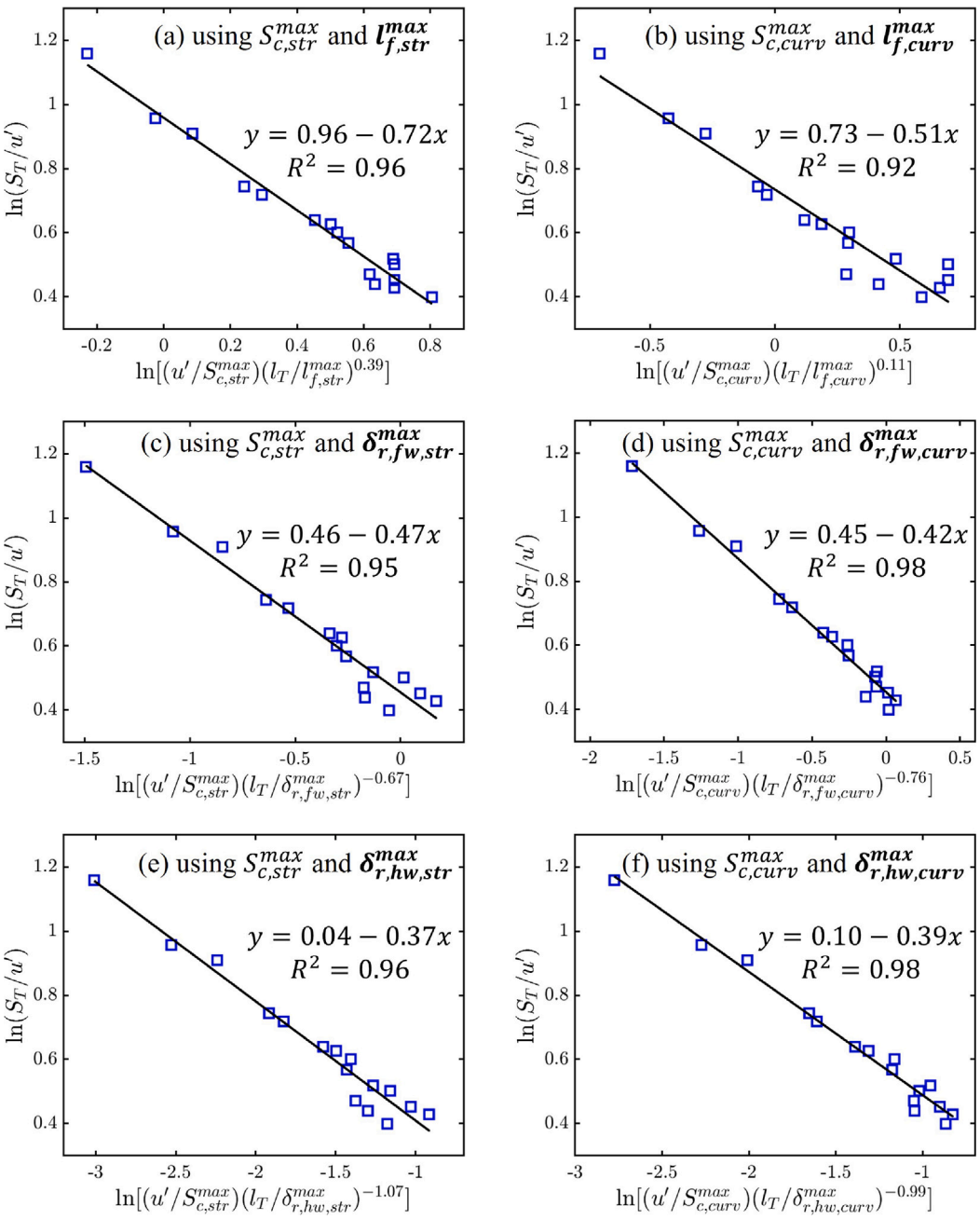

Fig. 15. All DNS S_T data fitted using Eq. (5) with $S_{c,str}^{max}$ and $l_{f,str}^{max}$ (left column) and $S_{c,curv}^{max}$ and $l_{f,curv}^{max}$ (right column). Plots placed in different rows show results obtained using different flame thicknesses specified in each plot.

data on S_T, are independent on turbulence characteristics, but vary with variations in mixture composition, pressure, and unburned gas temperature.

CRediT authorship contribution statement

Yiqing Wang: Writing – original draft, Methodology, Formal analysis, Conceptualization. **Andrei N. Lipatnikov:** Writing – review & editing, Supervision, Methodology, Conceptualization. **Zheng Chen:** Writing – review & editing, Supervision, Funding acquisition.

Declaration of competing interest

The authors declare that they have no known competing financial interests or personal relationships that could have appeared to influence the work reported in this paper.

The author is an Editorial Board Member/Editor-in-Chief/Associate Editor/Guest Editor for this journal and was not involved in the editorial review or the decision to publish this article.

Acknowledgments

This work was supported by the National Natural Science Foundation of China (No. 52425604). AL gratefully acknowledges support from Swedish Research Council (grant No. 2023-04407).

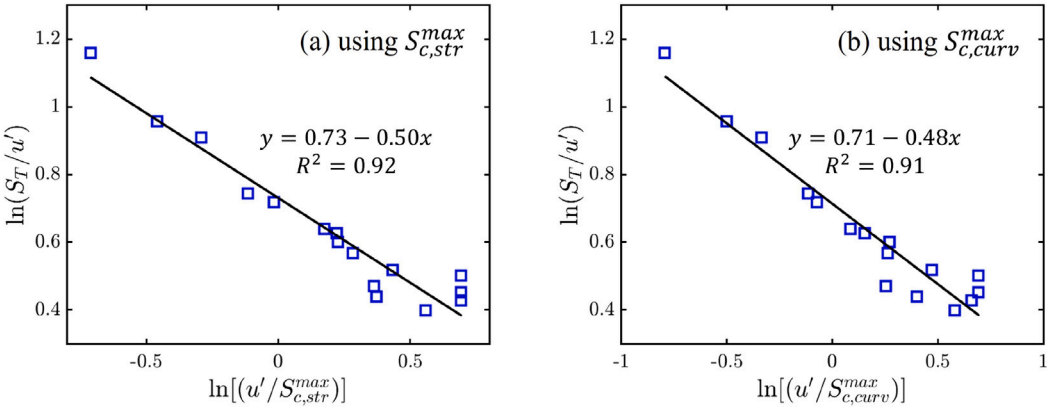

Fig. 16. All DNS S_T data fitted using Eqs. (7) and (8), respectively.

Appendix A. Supplementary data

Supplementary material related to this article can be found online at https://doi.org/10.1016/j.combustflame.2025.114306.

References

[1] J. Hwang, K. Maharjan, H. Cho, A review of hydrogen utilization in power generation and transportation sectors: Achievements and future challenges, Int. J. Hydrog. Energy 48 (74) (2023) 28629–28648.

[2] S. Manigandan, T. Praveenkumar, J.I. Ryu, T.N. Verma, A. Pugazhendhi, Role of hydrogen on aviation sector: A review on hydrogen storage, fuel flexibility, flame stability, and emissions reduction on gas turbines engines, Fuel 352 (2023) 129064.

[3] V.P. Karpov, A.S. Sokolik, Inflammation limits in turbulized gas mixtures, Dokl. Akad. Nauk SSSR 141 (2) (1961) 393–396.

[4] V.P. Karpov, E.S. Severin, Effects of molecular-transport coefficients on the rate of turbulent combustion, Combust. Explos. Shock. Waves 16 (1) (1980) 41–46.

[5] A.N. Lipatnikov, J. Chomiak, Molecular transport effects on turbulent flame propagation and structure, Prog. Energy Combust. Sci. 31 (1) (2005) 1–73.

[6] S. Yang, A. Saha, W. Liang, F. Wu, C.K. Law, Extreme role of preferential diffusion in turbulent flame propagation, Combust. Flame 188 (2018) 498–504.

[7] A.N. Lipatnikov, Y.-R. Chen, S. Shy, An experimental study of the influence of Lewis number on turbulent flame speed at different pressures, Proc. Combust. Inst. 39 (2) (2023) 2339–2347.

[8] S. Hochgreb, How fast can we burn, 2.0, Proc. Combust. Inst. 39 (2) (2023) 2077–2105.

[9] H. Pitsch, The transition to sustainable combustion: Hydrogen-and carbon-based future fuels and methods for dealing with their challenges, Proc. Combust. Inst. 40 (1–4) (2024) 105638.

[10] S. Daniele, P. Jansohn, J. Mantzaras, K. Boulouchos, Turbulent flame speed for syngas at gas turbine relevant conditions, Proc. Combust. Inst. 33 (2) (2011) 2937–2944.

[11] S. Daniele, J. Mantzaras, P. Jansohn, A. Denisov, K. Boulouchos, Flame front/turbulence interaction for syngas fuels in the thin reaction zones regime: turbulent and stretched laminar flame speeds at elevated pressures and temperatures, J. Fluid Mech. 724 (2013) 36–68.

[12] P. Venkateswaran, A. Marshall, D. Shin, D. Noble, J. Seitzman, T. Lieuwen, Measurements and analysis of turbulent consumption speeds of H_2/CO mixtures, Combust. Flame 158 (1) (2011) 1602–1614.

[13] P. Venkateswaran, A. Marshall, J. Seitzman, T. Lieuwen, Pressure and fuel effects on turbulent consumption speeds of h_2/CO blends, Proc. Combust. Inst. 34 (1) (2013) 1527–1535.

[14] P. Venkateswaran, A. Marshall, J. Seitzman, T. Lieuwen, Scaling turbulent flame speeds of negative Markstein length fuel blends using leading points concepts, Combust. Flame 162 (2) (2015) 375–387.

[15] L. Berger, A. Attili, H. Pitsch, Synergistic interactions of thermodiffusive instabilities and turbulence in lean hydrogen flames, Combust. Flame (ISSN: 0010-2180) 244 (2022) 112254.

[16] H.-C. Lee, P. Dai, M. Wan, A.N. Lipatnikov, A numerical support of leading point concept, Int. J. Hydrog. Energy 47 (55) (2022) 23444–23461.

[17] H. Lee, P. Dai, M. Wan, A.N. Lipatnikov, Displacement speed, flame surface density and burning rate in highly turbulent premixed flames characterized by low Lewis numbers, J. Fluid Mech. 961 (2023) A21.

[18] T. Howarth, E. Hunt, A. Aspden, Thermodiffusively-unstable lean premixed hydrogen flames: Phenomenology, empirical modelling, and thermal leading points, Combust. Flame 253 (2023) 112811.

[19] V. Coulon, J. Gaucherand, V. Xing, D. Laera, C. Lapeyre, T. Poinsot, Direct numerical simulations of methane, ammonia-hydrogen and hydrogen turbulent premixed flames, Combust. Flame 256 (2023) 112933.

[20] M. Rieth, A. Gruber, J.H. Chen, The effect of pressure on lean premixed hydrogen-air flames, Combust. Flame 250 (2023) 112514.

[21] H.-Y. Hsieh, S.M. Mousavi, A.N. Lipatnikov, S.S. Shy, Experimental study of the influence of lewis number, laminar flame thickness, temperature, and pressure on turbulent flame speed using hydrogen and methane fuels, Proc. Combust. Inst. 40 (1–4) (2024) 105752.

[22] T. Howarth, A. Aspden, An empirical characteristic scaling model for freely-propagating lean premixed hydrogen flames, Combust. Flame 237 (2022) 111805.

[23] M. Matalon, C. Cui, J. Bechtold, Hydrodynamic theory of premixed flames: effects of stoichiometry, variable transport coefficients and arbitrary reaction orders, J. Fluid Mech. 487 (2003) 179–210.

[24] E. Hunt, A. Aspden, Thermodiffusively-unstable lean premixed hydrogen flames: Length scale effects and turbulent burning regimes, Combust. Flame 272 (1) (2025) 113855.

[25] F.M. Ramirez, Q. Douasbin, O. Dounia, O. Vermorel, T. Jaravel, Flame-turbulence interactions in lean hydrogen flames: Implications for turbulent flame speed and fractal modelling, Combust. Flame 273 (1) (2025) 113926.

[26] D. Bradley, A. Lau, M. Lawes, Flame stretch rate as a determinant of turbulent burning velocity, Phil. Trans. R. Soc. A 338 (1650) (1992) 359–387.

[27] T. Kitagawa, T. Nakahara, K. Maruyama, K. Kado, A. Hayakawa, S. Kobayashi, Turbulent burning velocity of hydrogen–air premixed propagating flames at elevated pressures, Int. J. Hydrog. Energy 33 (20) (2008) 5842–5849.

[28] M. Nguyen, D. Yu, S. Shy, General correlations of high pressure turbulent burning velocities with the consideration of Lewis number effect, Proc. Combust. Inst. 37 (2) (2019) 2391–2398.

[29] S. Wang, A.M. Elbaz, O.Z. Arab, W.L. Roberts, Turbulent flame speed measurement of NH_3/H_2/air and CH_4/air flames and a numerical case study of NO emission in a constant volume combustion chamber (CVCC), Fuel 332 (2023) 126152.

[30] X. Cai, Q. Fan, X.-S. Bai, J. Wang, M. Zhang, Z. Huang, M. Aldén, Z. Li, Turbulent burning velocity and its related statistics of ammonia-hydrogen-air jet flames at high Karlovitz number: Effect of differential diffusion, Proc. Combust. Inst. 39 (4) (2023) 4215–4226.

[31] Y.B. Zeldovich, G.I. Barenblatt, V.B. Librovich, G.M. Makhviladze, The Mathematical Theory of Combustion and Explosions, Springer, 1985.

[32] V.R. Kuznetsov, V.A. Sabel'nikov, Turbulence and Combustion, Hemisphere Publishing Corporation, New York, 1990.

[33] W. Zhang, J. Wang, Q. Yu, W. Jin, M. Zhang, Z. Huang, Investigation of the fuel effects on burning velocity and flame structure of turbulent premixed flames based on leading points concept, Combust. Sci. Technol. 190 (8) (2018) 1354–1376.

[34] Z. Wang, X. Li, T. Li, A. Dreizler, S. Mousavi, A. Lipatnikov, B. Zhou, Experimental investigation of NH_3-H_2 jet flames adopting multi-scalar imaging: Comparison of turbulent burning velocities obtained using different flame-front markers, Combust. Flame 275 (1) (2025) 114054.

[35] H.-C. Lee, P. Dai, M. Wan, A.N. Lipatnikov, Influence of molecular transport on burning rate and conditioned species concentrations in highly turbulent premixed flames, J. Fluid Mech. 928 (2021) A5.

[36] H.-C. Lee, P. Dai, M. Wan, A.N. Lipatnikov, A DNS study of extreme and leading points in lean hydrogen-air turbulent flames – Part I: Local thermochemical structure and reaction rates, Combust. Flame (ISSN: 0010-2180) 235 (2022) 111716.

[37] H.-C. Lee, P. Dai, M. Wan, A.N. Lipatnikov, A DNS study of extreme and leading points in lean hydrogen-air turbulent flames – Part II: Local velocity field and flame topology, Combust. Flame 235 (2022) 111712.

[38] H.-C. Lee, A. Abdelsamie, P. Dai, M. Wan, A.N. Lipatnikov, Influence of equivalence ratio on turbulent burning velocity and extreme fuel consumption rate in lean hydrogen-air turbulent flames, Fuel 327 (2022) 124969.
[39] S. Verma, F. Monnier, A.N. Lipatnikov, Validation of leading point concept in RANS simulations of highly turbulent lean syngas-air flames with well-pronounced diffusional-thermal effects, Int. J. Hydrog. Energy 46 (13) (2021) 9222–9233.
[40] A.N. Lipatnikov, J. Chomiak, Lewis number effects in premixed turbulent combustion and highly perturbed laminar flames, Combust. Sci. Technol. 137 (1–6) (1998) 277–298.
[41] V.P. Karpov, A.N. Lipatnikov, V.L. Zimont, A test of an engineering model of premixed turbulent combustion, Proc. Combust. Inst. 26 (1) (1996) 249–257.
[42] Y. Wang, C. Xu, C. Chi, Y. Yang, Z. Chen, Temperature effect on turbulent burning velocity of lean premixed hydrogen/air flames, Phys. Fluids 36 (12) (2024) 125165.
[43] A. Kéromnès, W.K. Metcalfe, K.A. Heufer, N. Donohoe, A.K. Das, C.-J. Sung, J. Herzler, C. Naumann, P. Griebel, O. Mathieu, et al., An experimental and detailed chemical kinetic modeling study of hydrogen and syngas mixture oxidation at elevated pressures, Combust. Flame 160 (6) (2013) 995–1011.
[44] R. Borghi, Turbulent combustion modelling, Prog. Energy Combust. Sci. 14 (4) (1988) 245–292.
[45] N. Peters, Turbulent Combustion, Cambridge University Press, 2000.
[46] A. Aspden, M. Day, J. Bell, Towards the distributed burning regime in turbulent premixed flames, J. Fluid Mech. 871 (2019) 1–21.
[47] L. Berger, A. Attili, M. Gauding, H. Pitsch, Effects of Karlovitz number variations on thermodiffusive instabilities in lean turbulent hydrogen jet flames, Proc. Combust. Inst. 40 (1–4) (2024) 105219.
[48] D. Goodwin, H. Moffat, R. Speth, Cantera, 2015, http://www.cantera.org.
[49] S.M. Mousavi, A.N. Lipatnikov, Are differential diffusion effects of importance when burning hydrogen under elevated pressures and temperatures? Int. J. Hydrog. Energy 49 (2024) 1048–1058.
[50] S.M. Mousavi, A.N. Lipatnikov, Dependence of Zel'dovich number on pressure and temperature in lean hydrogen-air mixtures, Proc. Combust. Inst. 40 (1–4) (2024) 105501.
[51] Z. Chen, M.P. Burke, Y. Ju, Effects of Lewis number and ignition energy on the determination of laminar flame speed using propagating spherical flames, Proc. Combust. Inst. 32 (1) (2009) 1253–1260.
[52] Z. Chen, M.P. Burke, Y. Ju, Effects of compression and stretch on the determination of laminar flame speeds using propagating spherical flames, Combust. Theor. Model. 13 (2) (2009) 343–364.
[53] A.N. Lipatnikov, J. Chomiak, Turbulent flame speed and thickness: phenomenology, evaluation, and application in multi-dimensional simulations, Prog. Energy Combust. Sci. 28 (2) (2002) 1–73.